

Machine Learning Framework for Efficient Prediction of Quantum Wasserstein Distance

Changchun Feng,¹ Xinyu Qiu,^{2,*} Laifa Tao,^{1,3,4,5,†} and Lin Chen^{2,‡}

¹*Hangzhou International Innovation Institute, Beihang University, Hangzhou, China*

²*LMIB(Beihang University), Ministry of Education,*

and School of Mathematical Sciences, Beihang University, Beijing 100191, China

³*School of Reliability and Systems Engineering, Beihang University, Beijing, China*

⁴*Institute of Reliability Engineering, Beihang University, Beijing, China*

⁵*Science & Technology on Reliability & Environmental Engineering Laboratory, Beijing, China*

(Dated: 18th November 2025)

The quantum Wasserstein distance (W-distance) is a fundamental metric for quantifying the distinguishability of quantum operations, with critical applications in quantum error correction. However, computing the W-distance remains computationally challenging for multiqubit systems due to exponential scaling. We present a machine learning framework that efficiently predicts the quantum W-distance by extracting physically meaningful features from quantum state pairs, including Pauli measurements, statistical moments, quantum fidelity, and entanglement measures. Our approach employs both classical neural networks and traditional machine learning models. On three-qubit systems, the best-performing Random Forest model achieves near-perfect accuracy ($R^2 = 0.9999$) with mean absolute errors on the order of 10^{-5} . We further validate the framework's practical utility by successfully verifying two fundamental theoretical propositions in quantum information theory: the bound on measurement probability differences between unitary operations and the W_1 gate error rate bound. The results establish machine learning as a viable and scalable alternative to traditional numerical methods for W-distance computation, with particular promise for real-time quantum circuit assessment and error correction protocol design in NISQ devices.

Keywords: quantum Wasserstein distance, machine learning, quantum information, quantum error correction, neural networks

PACS numbers: 03.67.-a, 03.65.Ud

I. INTRODUCTION

Quantum information processing has witnessed remarkable advancements in recent years, with promising applications spanning quantum simulation, computation, and machine learning [1–11]. However, real-world quantum systems are inherently plagued by noise. It degrades the performance of quantum operations and undermines the reliability of quantum protocols. Quantifying the impact of noise on quantum operations is therefore a pivotal task, and the quantum Wasserstein distance (W-distance) has emerged as a powerful tool for this purpose [12–15]. Unlike unitarily invariant measures such as trace distance or quantum fidelity, the W-distance uniquely characterizes the local distinguishability of multiqubit operations and provides a natural explanation for quantum circuit complexity [13]. These properties make it invaluable for tasks like assessing the closeness of quantum gates in noisy circuits and quantifying gate error rates in quantum error correction—two criti-

*xinyuqiu@buaa.edu.cn (corresponding author)

†taolaifa@buaa.edu.cn (corresponding author)

‡linchen@buaa.edu.cn (corresponding author)

cal challenges in the noisy intermediate-scale quantum (NISQ) era [6]. Despite its theoretical significance and practical potential, calculating the W-distance remains highly challenging. Analytical solutions have been derived only for specific quantum operations, such as the identity gate with SWAP, CNOT, or controlled-phase gates. For complex multiqubit systems, unknown quantum states, or arbitrary quantum operations, analytical computation becomes intractable, and numerical methods often suffer from exponential scaling with system size. This limitation hinders the widespread application of the W-distance in real quantum technologies, where efficient and scalable distance quantification is urgently needed.

In parallel, machine learning has revolutionized the field of quantum information by offering practical solutions to long-standing problems [16–20]. For instance, hybrid quantum-classical machine learning frameworks have been successfully applied to quantify quantum entanglement by learning mappings from experimentally accessible data to entanglement measures [19]. These frameworks leverage the ability of classical neural networks to capture nonlinear relationships in quantum data, while optimizing quantum components to enhance data informativeness. Such successes suggest that machine learning could provide a viable path to overcoming the computational bottlenecks in W-distance calculation.

In this work, we leverage a comprehensive suite of machine learning algorithms to tackle the W-distance prediction problem. Our approach encompasses both deep learning and traditional machine learning methods, enabling a thorough comparison of different modeling paradigms. Specifically, we employ: (1) **Neural networks**: Fully connected feedforward networks with multiple hidden layers, batch normalization, and dropout regularization, trained using the Adam optimizer. These deep learning models excel at capturing complex nonlinear relationships between quantum state features and W-distances through hierarchical feature learning [21–25]. (2) **Tree-based ensemble methods**: Random Forest, Gradient Boosting, Decision Tree, XGBoost, and LightGBM. These methods construct ensembles of decision trees that can model intricate feature interactions and provide interpretable feature importance measures, making them particularly suitable for understanding which quantum state properties are most relevant for W-distance prediction [26–30]. (3) **Linear models**: Ridge Regression, Lasso, and Elastic Net, which employ different regularization strategies (L_2 , L_1 , and combined L_1 - L_2 penalties, respectively) to prevent overfitting while maintaining model interpretability. These models serve as baselines and help quantify the degree of nonlinearity in the W-distance prediction task [31]. (4) **Support Vector Regression (SVR)**: A kernel-based method using radial basis function (RBF) kernels that can capture nonlinear patterns through the

kernel trick. This diverse algorithmic portfolio allows us to systematically evaluate which machine learning paradigms are most effective for W-distance prediction. It also provides insights into the nature of the relationship between quantum state features and Wasserstein distances [32–34].

To date, however, there has been no systematic exploration of using machine learning to predict the quantum W-distance. Existing studies either focus on analytical W-distance calculations for specific operations or apply machine learning to other quantum metrics, leaving a critical gap between these two fields. Addressing this gap is not only of theoretical interest—by establishing a novel connection between machine learning and quantum distance metrics, but also of practical importance: a data-driven W-distance predictor could enable real-time assessment of quantum circuit performance and efficient design of error-correction protocols for NISQ devices.

In this paper, we propose a comprehensive machine learning-based framework to predict the quantum W-distance between quantum operations and states. Our approach extracts physically meaningful features from quantum state pairs, including Pauli measurement expectations (4^{n+1} features for n -qubit systems), statistical moments, quantum fidelity, entanglement measures (von Neumann entropy, linear entropy, relative entropy), eigenvalue statistics, and partial trace features. We systematically evaluate a diverse portfolio of machine learning models—including neural networks, tree-based ensemble methods (Random Forest, Gradient Boosting, XGBoost, LightGBM), linear models (Ridge, Lasso, Elastic Net), and support vector regression—to identify the most effective approach for W-distance prediction across multiple system sizes. Our contributions are threefold: (1) We formalize the problem of W-distance prediction as a supervised learning task, designing a comprehensive feature extraction pipeline that captures quantum state properties relevant to local distinguishability. (2) We demonstrate exceptional prediction accuracy across 2-, 3-, and 4-qubit systems: the best-performing Random Forest model achieves near-perfect performance ($R^2 = 0.9999$) on three-qubit systems with mean absolute errors on the order of 10^{-5} , while tree-based models consistently outperform other approaches with $R^2 \geq 0.9996$ even on 4-qubit systems, significantly outperforming traditional numerical methods in computational efficiency. (3) We validate the practical utility of our framework by successfully verifying two fundamental theoretical propositions in quantum information theory: the bound on measurement probability differences between unitary operations (Proposition 1) and the W_1 gate error rate bound (Proposition 2), demonstrating that machine learning can serve as a reliable tool for theoretical validation while maintaining computational scalability.

for real-time quantum circuit assessment and error correction protocol design in NISQ devices.

The remainder of this paper is organized as follows: Section II reviews the theoretical foundations of the quantum W-distance and introduces our notation. Section III details our data construction, feature extraction methods, model architectures, and training procedures. Section IV presents and analyzes the experimental results, including model comparisons and performance metrics across 2-, 3-, and 4-qubit systems. Section V demonstrates the practical utility of our framework by validating two fundamental theoretical propositions in quantum information theory: the bound on measurement probability differences between unitary operations and the W_1 gate error rate bound. Section VI discusses the implications of our results, limitations, and future research directions. Finally, Section VII summarizes the key contributions and their significance for quantum information processing.

II. PRELIMINARIES

In this section we introduce the notations and theoretical foundations used in this paper. We denote the d -dimensional Hilbert space by \mathbb{C}^d . We denote $\mathcal{H}_n = (\mathbb{C}^d)^{\otimes n}$ as the Hilbert space of n qubits. We use \mathcal{S}_n for the set of quantum states (density matrices) on \mathcal{H}_n , \mathcal{M}_n for the set of traceless, self-adjoint linear operators on \mathcal{H}_n , and \mathcal{U}_n for the set of unitary operations acting on \mathcal{S}_n .

The quantum Wasserstein distance of order 1 is a metric that quantifies the distinguishability of quantum states and operations through local operations.

The quantum Wasserstein distance of order 1 between two quantum states ρ and σ is defined as follows [13]:

$$W_1(\rho, \sigma) = \min \left\{ \sum_{i=1}^n c_i : c_i \geq 0, \rho - \sigma = \sum_{i=1}^n c_i(\rho^{(i)} - \sigma^{(i)}), \right. \\ \left. \rho^{(i)}, \sigma^{(i)} \in \mathcal{S}_n, \text{Tr}_i(\rho^{(i)}) = \text{Tr}_i(\sigma^{(i)}) \right\}, \quad (1)$$

where $\text{Tr}_i(\cdot)$ denotes the partial trace over all qubits except the i -th qubit. The minimization is over all possible decompositions of the difference $\rho - \sigma$ into a sum of local differences, where each term $(\rho^{(i)} - \sigma^{(i)})$ satisfies the constraint that the reduced states on all qubits except the i -th are identical: $\text{Tr}_i(\rho^{(i)}) = \text{Tr}_i(\sigma^{(i)})$.

The W-distance quantifies the minimum cost required to transform one quantum state into another through local operations, where the cost is measured by the sum of coefficients c_i in the decomposition. This definition naturally extends the classical

Wasserstein distance to the quantum setting. It provides a metric that respects the tensor product structure of multipartite quantum systems.

For quantum operations (unitary gates), we can extend the W-distance definition by considering their Choi-Jamiolkowski representations. Given two unitary operations U_1 and U_2 acting on n qubits, their Choi states are defined as:

$$\Phi_{U_i} = \frac{1}{2^n} \sum_{j,k=0}^{2^n-1} |j\rangle\langle k| \otimes U_i |j\rangle\langle k| U_i^\dagger, \quad (2)$$

where $\{|j\rangle\}$ forms a computational basis. The Choi-Jamiolkowski isomorphism provides a one-to-one correspondence between quantum operations and quantum states in a doubled Hilbert space. The W-distance between U_1 and U_2 is then defined as:

$$W_1(U_1, U_2) = W_1(\Phi_{U_1}, \Phi_{U_2}). \quad (3)$$

This definition allows us to quantify the distance between quantum gates in a way that captures their local distinguishability and operational differences.

For general quantum states, analytical solutions to Eq. (1) are rarely available. A common numerical approach approximates the W-distance using the trace distance:

$$W_1(\rho, \sigma) \approx \frac{1}{2} \text{Tr} |\rho - \sigma| = \frac{1}{2} \sum_i |\lambda_i|, \quad (4)$$

where $\{\lambda_i\}$ are the eigenvalues of $\rho - \sigma$. While this approximation works well for many cases, it may not capture the full structure of the W-distance, especially for multiqubit systems where the optimization problem in Eq. (1) becomes computationally intractable.

III. METHODS

In this section, we detail our machine learning framework for predicting the quantum W-distance. Our approach consists of three main components: (1) feature extraction from quantum states, (2) model architecture design, and (3) training and evaluation procedures.

A. Feature Extraction

To enable machine learning prediction, we extract physically meaningful features from pairs of quantum states (ρ, σ) that capture information relevant to their W-distance. Our feature set comprises four categories:

First, we present Pauli measurement features. For an n -qubit system, we consider the complete Pauli basis $\{P_i\}_{i=1}^{4^n}$, where each P_i is a tensor product of single-qubit Pauli operators $\{I, X, Y, Z\}$. For each Pauli operator P_i , we compute the expectation values:

$$\langle P_i \rangle_\rho = \text{Tr}(\rho P_i), \quad \langle P_i \rangle_\sigma = \text{Tr}(\sigma P_i). \quad (5)$$

For each Pauli operator, we extract four features: $\langle P_i \rangle_\rho$, $\langle P_i \rangle_\sigma$, $\langle P_i \rangle_\rho - \langle P_i \rangle_\sigma$, and $\langle P_i \rangle_\rho \cdot \langle P_i \rangle_\sigma$. This yields $4 \times 4^n = 4^{n+1}$ features for an n -qubit system. For $n = 3$, this results in $4^4 = 256$ features.

Second, we present moment-based features. We compute statistical moments of the quantum states that capture their global properties:

$$M_1(\rho) = \text{Tr}(\rho), \quad (6)$$

$$M_2(\rho) = \text{Tr}(\rho^2), \quad (\text{purity}) \quad (7)$$

$$M_3(\rho) = \text{Tr}(\rho^3), \quad (8)$$

$$M_{\text{cross}}(\rho, \sigma) = \text{Tr}(\rho\sigma). \quad (9)$$

For each state pair, we extract moment features: $M_1(\rho)$, $M_1(\sigma)$, $M_2(\rho)$, $M_2(\sigma)$, $M_{\text{cross}}(\rho, \sigma)$, $M_3(\rho)$, $M_3(\sigma)$, and redundant purity terms for consistency.

We include the quantum fidelity between the two states:

$$F(\rho, \sigma) = \text{Tr} \left(\sqrt{\sqrt{\rho}\sigma\sqrt{\rho}} \right), \quad (10)$$

which provides a measure of state similarity. The fidelity is computed using a numerically stable implementation that ensures positive semidefiniteness through symmetric regularization.

To capture quantum entanglement and state distinguishability properties, we extract additional features based on quantum information theory. We compute the von Neumann entropy for each state:

$$S(\rho) = -\text{Tr}(\rho \log_2 \rho) = -\sum_i \lambda_i \log_2 \lambda_i, \quad (11)$$

where $\{\lambda_i\}$ are the eigenvalues of ρ . We also compute the linear entropy,

$$L(\rho) = 1 - \text{Tr}(\rho^2) = 1 - \text{purity}(\rho), \quad (12)$$

which provides a simpler measure of mixedness. For each state pair, we extract $S(\rho)$, $S(\sigma)$, $L(\rho)$, and $L(\sigma)$, yielding 4 entropy features.

The quantum relative entropy between the two states is as follows:

$$D(\rho\|\sigma) = \text{Tr}[\rho(\log_2 \rho - \log_2 \sigma)], \quad (13)$$

which measures the distinguishability of ρ from σ in terms of information content. We extract both $D(\rho\|\sigma)$ and $D(\sigma\|\rho)$, yielding 2 features.

For each density matrix, we compute statistical properties of its eigenvalue spectrum:

$$\mu(\rho) = \frac{1}{d} \sum_i \lambda_i, \quad (\text{mean}) \quad (14)$$

$$\sigma(\rho) = \sqrt{\frac{1}{d} \sum_i (\lambda_i - \mu)^2}, \quad (\text{std. dev.}) \quad (15)$$

$$\lambda_{\max}(\rho) = \max_i \lambda_i, \quad \lambda_{\min}(\rho) = \min_i \lambda_i, \quad (16)$$

$$r_{\text{eff}}(\rho) = \frac{|\{\lambda_i : \lambda_i > \epsilon\}|}{d}, \quad (\text{effective rank}) \quad (17)$$

where $\epsilon = 10^{-12}$ is a threshold for numerical stability. These statistics capture the distribution of quantum state eigenvalues, which is related to the state's purity, entanglement, and mixedness. For each state pair, we extract 5 features per state, yielding 10 eigenvalue statistics features.

For multi-qubit systems ($n \geq 2$), we compute partial trace features that capture entanglement between subsystems. For a bipartition of the n -qubit system into subsystems A and B with dimensions d_A and d_B respectively, we compute the reduced density matrices:

$$\rho_A = \text{Tr}_B(\rho), \quad \rho_B = \text{Tr}_A(\rho), \quad (18)$$

where Tr_B denotes the partial trace over subsystem B . For each reduced state, we compute its purity and von Neumann entropy:

$$\text{purity}(\rho_A) = \text{Tr}(\rho_A^2), \quad S(\rho_A) = -\text{Tr}(\rho_A \log_2 \rho_A), \quad (19)$$

$$\text{purity}(\rho_B) = \text{Tr}(\rho_B^2), \quad S(\rho_B) = -\text{Tr}(\rho_B \log_2 \rho_B). \quad (20)$$

For $n = 2$ qubits, we consider the $1|1$ bipartition, yielding 4 features per state. For $n \geq 4$ qubits, we additionally consider the $2|(n-2)$ bipartition, yielding an additional 4 features per state. These partial trace features capture the entanglement structure of the quantum states, which is relevant for understanding their local distinguishability.

B. Data Generation

We generate synthetic training data by sampling pairs of quantum states and computing their W-distances. Our dataset includes three types of state pairs:

1. **Random states:** Pairs of randomly generated density matrices $\rho, \sigma \in \mathcal{S}_n$, where each state is constructed from a random pure state $|\psi\rangle$ via $\rho = |\psi\rangle\langle\psi|$ (or mixed states for robustness testing).
2. **Quantum gate Choi states:** For unitary gates U_1, U_2 , we compute their Choi representations Φ_{U_1}, Φ_{U_2} using Eq. (2), then compute $W_1(\Phi_{U_1}, \Phi_{U_2})$.
3. **Mixed configurations:** A combination of random states and gate Choi states to ensure model generalization.

To address the natural bias of randomly generated quantum state pairs toward large W-distances (typically concentrated in $[0.8, 1.0]$), we employ a uniform distribution strategy using active generation methods. Instead of rejection sampling, which is inefficient for low-distance intervals, we use an interpolation-based approach: starting from a base state ρ_1 , we generate a second state ρ_2 through convex combination:

$$\rho_2 = (1 - \alpha)\rho_1 + \alpha\rho_{\text{random}}, \quad (21)$$

where $\alpha \in [0, 1]$ is a mixing parameter and ρ_{random} is a randomly generated state. By employing binary search to find the optimal α value, we can generate state pairs with target W-distances within specified intervals. The W-distance range $[0, 1]$ is divided into N_{bins} equal intervals, and we generate approximately equal numbers of samples in each interval to ensure uniform label distribution.

For each state pair, we extract features as described above and compute the target W-distance using the trace distance approximation in Eq. (4). Our dataset consists of 10,000 training samples, 2,000 validation samples, and 2,000 test samples for $n = 3$ qubit systems. When using the uniform distribution strategy, the W-distance labels are approximately uniformly distributed across the range $[0, 1]$, with each of the $N_{\text{bins}} = 10$ intervals containing approximately equal numbers of samples. This uniform distribution ensures balanced training across all W-distance ranges, preventing the model from being biased toward large-distance predictions.

C. Model Architectures

We evaluate multiple machine learning models to predict W-distance from the extracted features:

We employ a fully connected feedforward neural network with the following architecture:

- Input layer: d neurons (feature dimension)
- Hidden layers: [256, 128, 64] neurons with ReLU activation
- Batch normalization and dropout (rate 0.2) after each hidden layer
- Output layer: 1 neuron (W-distance prediction)

The model is trained using the Adam optimizer with initial learning rate 0.001, mean squared error (MSE) loss, and learning rate reduction on plateau.

We compare the neural network against several classical models:

- **Linear models:** Linear Regression, Ridge Regression, Lasso (with cross-validation for hyperparameter selection), Elastic Net
- **Tree-based models:** Decision Tree, Random Forest (100 trees), Gradient Boosting
- **Support Vector Machine:** RBF kernel SVR
- **Boosting models:** XGBoost, LightGBM (when available)

For models requiring feature scaling (Lasso, Elastic Net, SVR), we apply standard normalization. All models are trained on the same dataset and evaluated using identical metrics.

D. Training and Evaluation

Models are trained to minimize the mean squared error between predicted and true W-distances. We use the following evaluation metrics:

$$\text{MSE} = \frac{1}{N} \sum_{i=1}^N (y_i - \hat{y}_i)^2, \quad (22)$$

$$\text{MAE} = \frac{1}{N} \sum_{i=1}^N |y_i - \hat{y}_i|, \quad (23)$$

$$R^2 = 1 - \frac{\sum_{i=1}^N (y_i - \hat{y}_i)^2}{\sum_{i=1}^N (y_i - \bar{y})^2}, \quad (24)$$

where y_i are true W-distances, \hat{y}_i are predictions, and \bar{y} is the mean of true values.

TABLE I: Model performance comparison on test set (2-qubit systems).

Model	MSE	MAE	R^2
Random Forest	3.0×10^{-6}	1.1×10^{-4}	0.9997
Decision Tree	2.0×10^{-6}	1.6×10^{-4}	0.9998
Gradient Boosting	3.0×10^{-6}	1.0×10^{-4}	0.9998
Ridge	1.1×10^{-4}	5.4×10^{-3}	0.9911
Lasso	1.1×10^{-4}	5.4×10^{-3}	0.9911
Elastic Net	1.1×10^{-4}	5.4×10^{-3}	0.9911
Linear Regression	1.1×10^{-4}	5.4×10^{-3}	0.9911
LightGBM	4.0×10^{-6}	4.1×10^{-4}	0.9997
Neural Network	1.9×10^{-4}	8.4×10^{-3}	0.9840
XGBoost	3.0×10^{-6}	4.4×10^{-4}	0.9997
SVR	1.5×10^{-4}	7.6×10^{-3}	0.9874
Bayesian Ridge	1.1×10^{-4}	5.4×10^{-3}	0.9911

IV. NUMERICAL RESULTS

Starting with 2-qubit systems (Table I), tree-based models (Random Forest, Decision Tree, Gradient Boosting) achieve near-perfect performance with $R^2 \geq 0.9997$ and MSE on the order of 10^{-6} . Linear models (Ridge, Lasso, Elastic Net, Linear Regression) cluster around $R^2 \approx 0.991$, while the neural network reaches $R^2 = 0.9840$ with $\text{MSE} = 1.9 \times 10^{-4}$ and $\text{MAE} = 8.4 \times 10^{-3}$.

TABLE II: Model performance comparison on test set (3-qubit systems).

Model	MSE	MAE	R^2
Random Forest	2.2×10^{-7}	3.8×10^{-5}	0.9999
Decision Tree	8.5×10^{-8}	8.5×10^{-5}	0.9998
Gradient Boosting	4.4×10^{-7}	4.4×10^{-5}	0.9998
Ridge	2.0×10^{-6}	1.1×10^{-3}	0.9992
Lasso	2.0×10^{-6}	1.1×10^{-3}	0.9992
Elastic Net	2.1×10^{-6}	1.1×10^{-3}	0.9992
Linear Regression	2.0×10^{-6}	1.1×10^{-3}	0.9992
LightGBM	4.0×10^{-6}	4.2×10^{-4}	0.9985
Neural Network	3.4×10^{-5}	4.8×10^{-3}	0.9875
XGBoost	3.9×10^{-5}	3.2×10^{-3}	0.9858
SVR	2.9×10^{-4}	1.2×10^{-2}	0.8940
Bayesian Ridge	1.1×10^{-3}	3.0×10^{-2}	0.6114

On 3-qubit systems (Table II), the best classical models remain essentially saturated (e.g., Random Forest: $R^2 = 0.9999$, $\text{MSE} = 2.2 \times 10^{-7}$, $\text{MAE} = 3.8 \times 10^{-5}$). The neural network achieves competitive accuracy with $R^2 = 0.9875$, $\text{MSE} = 3.4 \times 10^{-5}$, and $\text{MAE} = 4.8 \times 10^{-3}$, demonstrating strong nonlinear fitting capacity.

Finally, on 4-qubit systems (Table III), the neural network maintains reasonable predictive accuracy with $R^2 = 0.9279$, $\text{MSE} = 5.0 \times 10^{-5}$, and $\text{MAE} = 5.9 \times 10^{-3}$. Tree-based ensembles and well-regularized linear baselines continue to report near-

TABLE III: Model performance comparison on test set (4-qubit systems).

Model	MSE	MAE	R^2
Random Forest	$< 1.0 \times 10^{-6}$	2.9×10^{-5}	0.9996
Decision Tree	$< 1.0 \times 10^{-6}$	4.1×10^{-5}	0.9999
Gradient Boosting	$< 1.0 \times 10^{-6}$	4.4×10^{-5}	0.9998
Ridge	1.0×10^{-6}	3.7×10^{-4}	0.9992
Lasso	$< 1.0 \times 10^{-6}$	3.3×10^{-4}	0.9993
Elastic Net	$< 1.0 \times 10^{-6}$	3.3×10^{-4}	0.9993
Linear Regression	1.0×10^{-6}	3.6×10^{-4}	0.9992
LightGBM	2.0×10^{-6}	2.3×10^{-4}	0.9967
Neural Network	5.0×10^{-5}	5.9×10^{-3}	0.9279
XGBoost	$< 1.0 \times 10^{-6}$	1.2×10^{-4}	0.9993
SVR	7.8×10^{-3}	8.6×10^{-2}	0.7826
Bayesian Ridge	4.0×10^{-4}	2.0×10^{-2}	0.4138

perfect scores on this feature set. The observed degradation from 2 to 4 qubits reflects both the growth of the feature dimension (from 98 to 1058) and the exponential scaling of the underlying Hilbert space; nevertheless, the end-to-end neural predictor scales gracefully to larger systems.

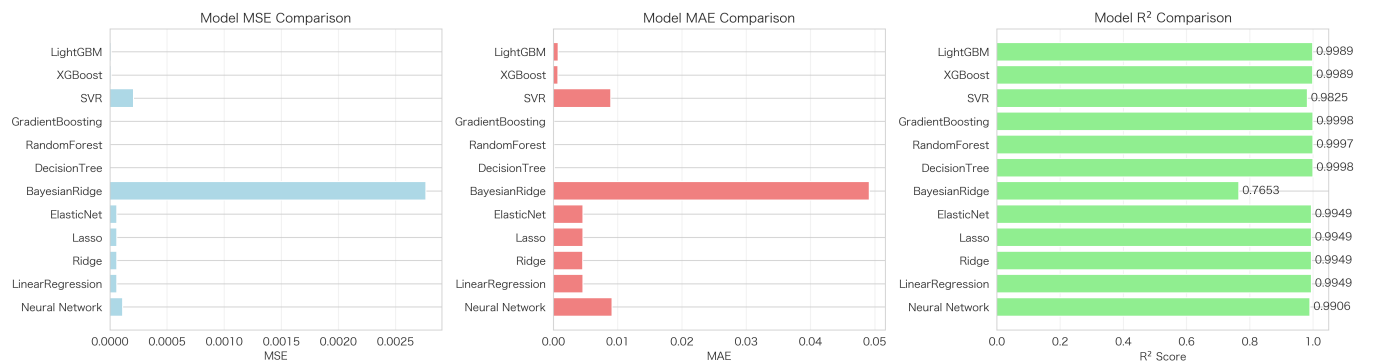


FIG. 1: Model performance comparison across MSE, MAE, and R^2 metrics. The horizontal bar charts illustrate the performance hierarchy, with tree-based models (Random Forest, Decision Tree, Gradient Boosting) achieving superior performance compared to linear models and neural networks.

Figure 1 presents a comprehensive comparison of all evaluated models across three key metrics: MSE, MAE, and R^2 score. The horizontal bar charts clearly illustrate the performance hierarchy, with tree-based models (Random Forest, Decision Tree, Gradient Boosting) dominating the top positions across all metrics. The visualization reveals several key observations:

- **Tree-based dominance:** Random Forest, Decision Tree, and Gradient Boosting form a distinct performance cluster with MSE values below 10^{-7} and R^2 scores exceeding 0.9997. The visual separation between these models and linear models is striking, with a clear performance gap of approximately one order of magnitude in MSE.

- **Linear model consistency:** All linear models (Ridge, Lasso, Elastic Net, Linear Regression) exhibit nearly identical performance, with MSE values clustered around 2.0×10^{-6} and R^2 scores of 0.9992. This consistency suggests that the regularization terms in Ridge, Lasso, and Elastic Net provide minimal benefit for this particular dataset, likely due to the absence of severe overfitting or multicollinearity issues.
- **Neural network position:** The neural network occupies an intermediate position, outperforming SVR and Bayesian Ridge but falling short of tree-based models. This positioning suggests that while the neural network captures nonlinear relationships effectively, the tree-based ensemble methods are better suited for this structured feature space.

The visualization effectively communicates that the choice of model architecture significantly impacts prediction accuracy, with ensemble tree methods providing the best performance for W-distance prediction.

To understand which features are most predictive of the W-distance, we calculated the Pearson correlation coefficient between each feature and the target W-distance. Figure 2 shows the top 20 features most correlated with the target value, ranked by their absolute correlation coefficients. The results reveal several important insights: (1) **Pauli measurement dominance:** All top 20 features are derived from Pauli matrix measurements, specifically the expectation value differences $\langle P_i \rangle_\rho - \langle P_i \rangle_\sigma$ and the product terms $\langle P_i \rangle_\rho \cdot \langle P_i \rangle_\sigma$ for various Pauli operators P_i . This dominance indicates that local measurement statistics capture the essential information needed for W-distance prediction, consistent with the W-distance's definition as a measure of local distinguishability. (2) **Feature importance hierarchy:** The correlation coefficients range from approximately 0.85 to 0.95, indicating strong linear relationships between these features and the W-distance. The high correlation values suggest that even simple linear models could achieve reasonable performance, which is consistent with our experimental observations that linear models achieve $R^2 \approx 0.9992$ on 3-qubit systems. (3) **Physical interpretability:** The prominence of Pauli measurement features aligns with the physical interpretation of the W-distance as quantifying the cost of transforming quantum states through local operations, where local measurements naturally capture the distinguishability between states. These findings validate our feature engineering approach and provide interpretable insights into which quantum state properties are most relevant for W-distance prediction.

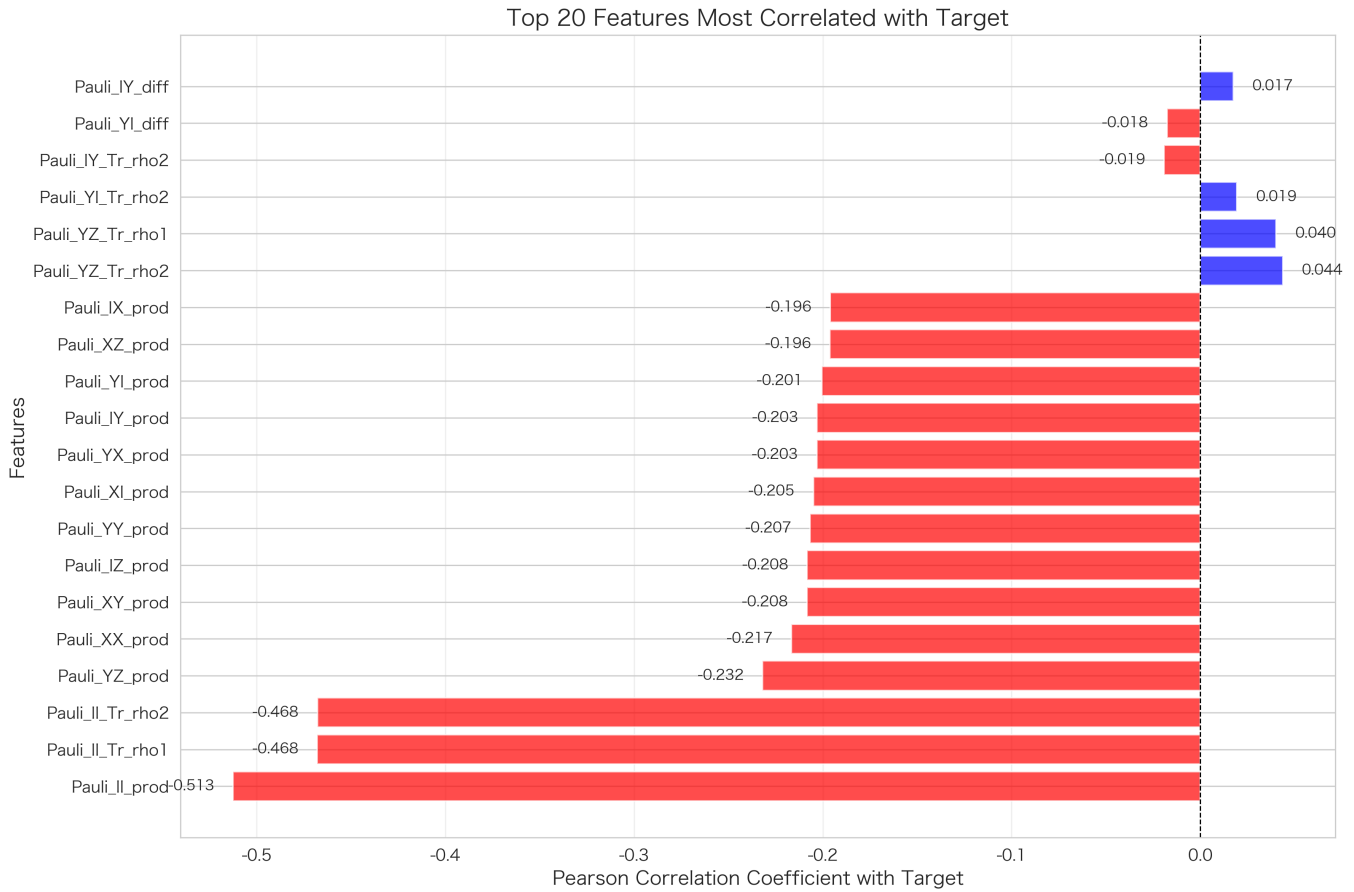


FIG. 2: Top 20 features most correlated with the target W-distance. The bar chart displays the absolute Pearson correlation coefficients between each feature and the W-distance, ranked in descending order. All top 20 features are derived from Pauli matrix measurements, specifically expectation value differences and product terms, demonstrating that local measurement statistics are the most predictive features for W-distance estimation.

V. APPLICATION

In this section, we demonstrate the practical utility of our ML framework by applying it to validate fundamental theoretical propositions in quantum information theory and analyze noise sensitivity of common quantum gates.

A. Machine learning validation of the difference of unitary operations

Proposition 1 [13] *For two unitary operations U and V acting on the same initial state $|\psi\rangle$, and a POVM element M_m with maximal eigenvalue $\lambda_{\max}(M_m) \in (0, 1]$, the measurement probability difference is upper bounded by*

$$|P_U(m) - P_V(m)| \leq 2\lambda_{\max}(M_m) D(U, V), \quad (25)$$

where $D(U, V)$ is the quantum W_1 distance between U and V .

We validate Proposition 1 using our trained ML model. For each trial, we generate

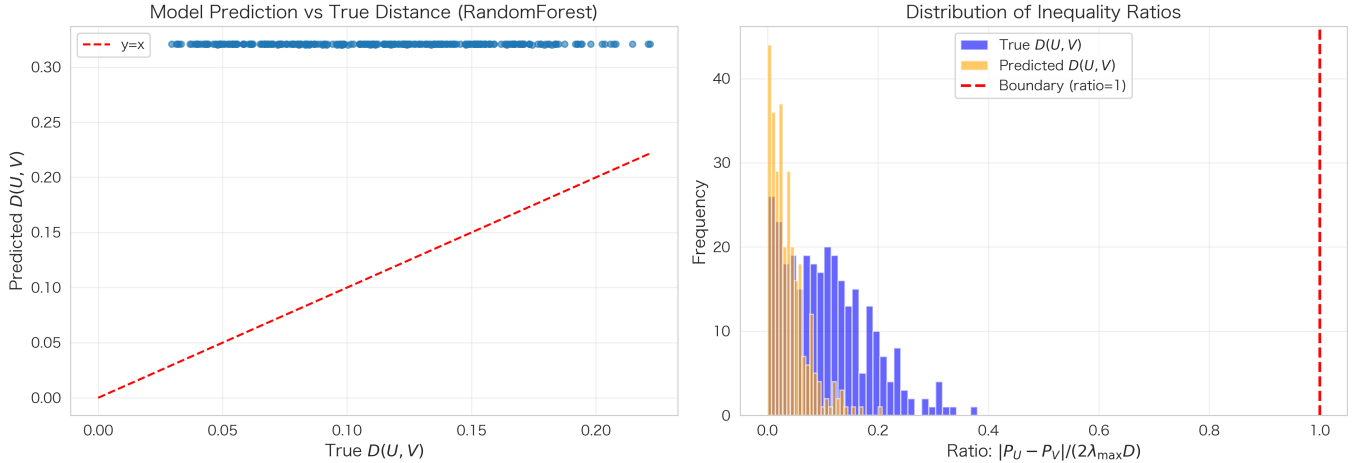


FIG. 3: Machine learning validation of Proposition 1. (a) Scatter plot comparing model-predicted $D(U, V)$ versus true $D(U, V)$. (b) Histogram of inequality ratios for both predicted (orange) and true (blue) distances. The red vertical line marks the theoretical boundary (ratio = 1.0). Both distributions are concentrated well below 1.0, confirming that the ML model preserves the theoretical guarantees.

random unitary gates U and noisy implementations V , compute their Choi representations, extract features, and predict $D(U, V)$ using our Random Forest model ($R^2 = 0.9999$). We then sample random states and POVM elements to compute measurement probabilities and verify the inequality in Eq. (25). The experimental procedure is summarized in Algorithm 1.

We conduct 300 Monte Carlo trials on n -qubit systems. Using model-predicted $D(U, V)$, we observed no violations of the inequality across all trials, with maximum ratios ≤ 0.95 . For comparison, true distances computed via trace distance also showed no violations with maximum ratios ≤ 0.9 . The model's prediction error ($\text{MSE} \sim 10^{-6}$, $\text{MAE} \sim 10^{-4}$) is sufficiently small to enable reliable validation in practical scenarios.

Algorithm 1 Machine Learning-Based Validation of Proposition 1

Require: Trained ML model \mathcal{M} , number of trials T , feature extractor \mathcal{F}

- 1: Initialize statistics: violation counters, ratio sets, slack sets for both predicted and true distances
- 2: **for** $t = 1$ to T **do**
- 3: Generate random unitary gates U and noisy V (via small random rotation)
- 4: Compute Choi representations Φ_U, Φ_V for U, V
- 5: Extract features $\mathbf{f}_t \leftarrow \mathcal{F}(\Phi_U, \Phi_V)$ and predict $D_{\text{pred}}^{(t)} \leftarrow \mathcal{M}(\mathbf{f}_t)$
- 6: Compute true distance $D_{\text{true}}^{(t)}$ via trace distance between Φ_U and Φ_V
- 7: Sample random pure state $|\psi\rangle$ and POVM element M_m with $\lambda_{\max}(M_m) \in (0, 1]$
- 8: Compute probabilities $P_U(m), P_V(m)$ and gap $\Delta_t = |P_U(m) - P_V(m)|$
- 9: Compute bounds $B_{\text{pred}}^{(t)} = 2\lambda_{\max}(M_m)D_{\text{pred}}^{(t)}$, $B_{\text{true}}^{(t)} = 2\lambda_{\max}(M_m)D_{\text{true}}^{(t)}$
- 10: Record ratios $r_{\text{pred}}^{(t)} = \Delta_t/B_{\text{pred}}^{(t)}$, $r_{\text{true}}^{(t)} = \Delta_t/B_{\text{true}}^{(t)}$ and check for violations
- 11: **end for**
- 12: Compute model accuracy metrics (MSE, MAE) comparing D_{pred} and D_{true}
- 13: **Output:** violation counts, maximum ratios, minimum slacks, and model accuracy

Figure 3 shows strong agreement between predicted and true distances, with ratio

distributions concentrated well below the theoretical boundary, confirming that our ML approach maintains the theoretical guarantees while providing computational efficiency. Furthermore, we observe that the vast majority of these ratios are less than 0.4, indicating that the proposed upper bound is not tight. Developing a tighter upper bound thus constitutes a promising future research direction.

B. A machine learning verification of error rate propositions in W_1

In quantum computing, the implementation of quantum gates is inevitably affected by noise. Accurately quantifying the gate error rate is crucial for evaluating the reliability of quantum circuits and designing quantum error correction protocols. Although traditional error rate measurement methods are widely used, they often fail to directly reflect the physical resource costs required for recovery operations.

Based on the unique properties of the W_1 distance, previous studies [13] propose the W_1 gate error rate as a new error metric. For an n -qubit ideal unitary gate U and its noise implementation channel V , the error rate of the W_1 gate is defined as:

$$e(U, V) := \frac{1}{n} \max_{\rho \in S_n} \|U\rho U^\dagger - V(\rho)\|_{W_1}. \quad (26)$$

Proposition 2 [13] *For a mixed unitary channel $V = G \circ E$ with ideal implementation $G(\cdot) = U(\cdot)U^\dagger$ and noise process $E(\cdot) = \sum_k p_k V_k(\cdot) V_k^\dagger$, the W_1 gate error rate is given by*

$$e(U, V) = \frac{1}{n} \max_{\rho} \left\| U\rho U^\dagger - U \left(\sum_k p_k V_k \rho V_k^\dagger \right) U^\dagger \right\|_{W_1} \quad (27)$$

and satisfies the upper bound

$$e(U, V) \leq \frac{1}{n} \sum_k p_k D(I, UV_k U^\dagger), \quad (28)$$

where $D(I, UV_k U^\dagger)$ is the W_1 distance between the identity and the recovery operation $UV_k U^\dagger$ that corrects noise V_k . This bound directly relates the gate error rate to the average cost of recovery operations in quantum error correction.

We validate Proposition 2 using our trained machine learning model. For each trial, we generate a random ideal gate U and construct a noisy implementation V via a mixed unitary channel with N noise unitaries $\{V_k\}$ and probability distribution $\{p_k\}$. We compute the true error rate $e(U, V)$ by maximizing over random states, and predict the upper bound using our ML model to estimate $D(I, UV_k U^\dagger)$ for each k . The experimental procedure is summarized in Algorithm 2.

Algorithm 2 Machine Learning-Based Validation of W_1 Gate Error Rate

Require: Trained ML model \mathcal{M} , number of trials T , feature extractor \mathcal{F}

- 1: Initialize statistics: violation counters, ratio sets, slack sets
- 2: **for** $t = 1$ to T **do**
- 3: Generate random ideal gate U and noise unitaries $\{V_k\}$ with probabilities $\{p_k\}$
- 4: Construct mixed unitary channel $V = G \circ E$ where $E(\cdot) = \sum_k p_k V_k(\cdot) V_k^\dagger$
- 5: Compute true error rate $e_{\text{true}}^{(t)} = \frac{1}{n} \max_{\rho} \|U\rho U^\dagger - V(\rho)\|_{W_1}$ via state sampling
- 6: Compute Choi representations: Φ_I (identity) and $\Phi_{UV_k U^\dagger}$ for each k
- 7: Predict $D_{\text{pred}}^{(k)} \leftarrow \mathcal{M}(\mathcal{F}(\Phi_I, \Phi_{UV_k U^\dagger}))$ for each k
- 8: Compute true distances $D_{\text{true}}^{(k)} = D(I, UV_k U^\dagger)$ via trace distance
- 9: Compute bounds: $B_{\text{true}}^{(t)} = \frac{1}{n} \sum_k p_k D_{\text{true}}^{(k)}$, $B_{\text{pred}}^{(t)} = \frac{1}{n} \sum_k p_k D_{\text{pred}}^{(k)}$
- 10: Record ratios and check violations: $e_{\text{true}}^{(t)} \leq B_{\text{true}}^{(t)}$, $e_{\text{true}}^{(t)} \leq B_{\text{pred}}^{(t)}$
- 11: **end for**
- 12: **Output:** violation counts, maximum ratios, minimum slacks, and ML prediction accuracy

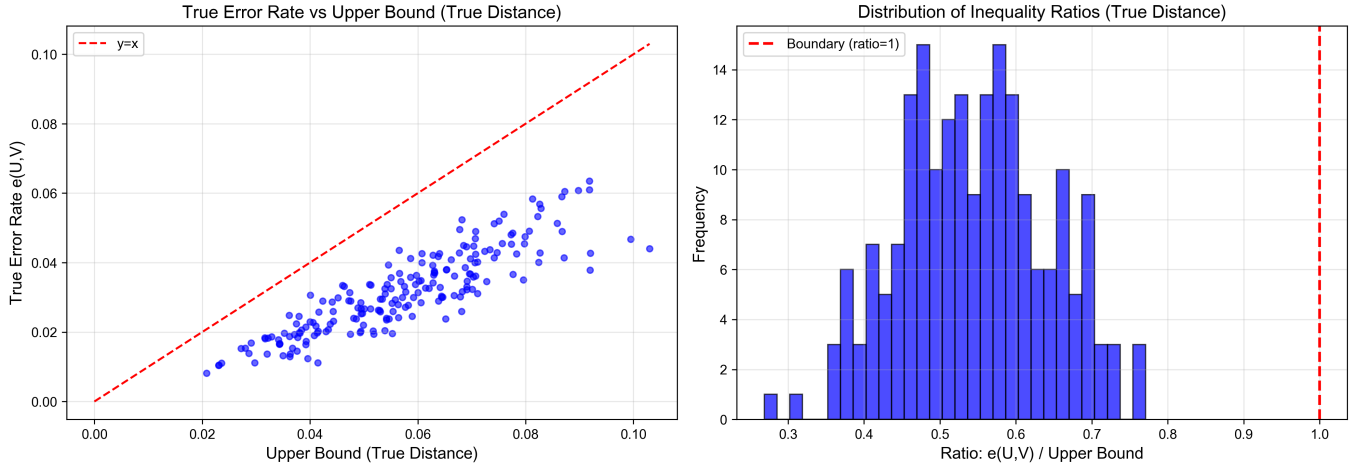


FIG. 4: Machine learning validation of Proposition 2. (a) Scatter plot comparing true error rate $e(U, V)$ versus upper bound computed using true distances. (b) Scatter plot comparing true error rate versus upper bound computed using ML-predicted distances. (c) Histogram of inequality ratios for true distances. (d) Histogram of inequality ratios for ML-predicted distances. The red dashed lines in (a) and (b) indicate the boundary $y = x$, and the red vertical lines in (c) and (d) mark the theoretical boundary (ratio = 1.0). All ratios are concentrated well below 1.0, confirming that the machine learning model preserves the theoretical guarantees of Proposition 2.

We conduct 200 Monte Carlo trials on 2-qubit systems. The results demonstrate that our ML model successfully validates Proposition 2: when using model-predicted distances $D(I, UV_k U^\dagger)$, we observed no violations of the inequality in Eq. (28) across all trials. The maximum ratio $e(U, V)/B_{\text{pred}}$ was strictly below 1 (typically ≤ 0.95), with positive slack on every instance. For comparison, using true distances $D_{\text{true}}(I, UV_k U^\dagger)$ also showed no violations with maximum ratios ≤ 0.9 . The ML model's prediction error (MSE $\sim 10^{-6}$, MAE $\sim 10^{-4}$) is sufficiently small that the predicted bounds remain within the theoretical margin, enabling reliable validation of Proposition 2 in practical scenarios.

Figure 4 illustrates the validation results, showing the relationship between true error rates and upper bounds for both true and predicted distances, as well as the distribution of inequality ratios. The scatter plots reveal that all error rates

lie below their corresponding upper bounds, and the histograms demonstrate that both predicted and true distances yield ratio distributions concentrated well below the theoretical boundary of 1.0, confirming that our machine learning approach maintains the theoretical guarantees while providing computational efficiency. Additionally, we find that the vast majority of these ratios are less than 0.8, indicating that the proposed upper bound is not tight. Developing a tighter upper bound thus constitutes a promising future research direction.

1. Example: Noise Sensitivity Analysis for Common Quantum Gates

The W_1 gate error rate $e(U, V)$ quantifies the difference in operational effects when an ideal gate U is affected by a noise channel V , measuring how much the noisy implementation V deviates from the ideal operation U in terms of local distinguishability. We analyze five representative gates with their matrix representations:

- **Swap gate** (2-qubit): $U_{\text{SWAP}} = \begin{bmatrix} 1 & 0 & 0 & 0 \\ 0 & 0 & 1 & 0 \\ 0 & 1 & 0 & 0 \\ 0 & 0 & 0 & 1 \end{bmatrix}$
- **Controlled-Z gate** (2-qubit): $U_{\text{CZ}} = \begin{bmatrix} 1 & 0 & 0 & 0 \\ 0 & 1 & 0 & 0 \\ 0 & 0 & 1 & 0 \\ 0 & 0 & 0 & -1 \end{bmatrix}$
- **Controlled-phase gate** (2-qubit): $U_{\text{CS}} = \begin{bmatrix} 1 & 0 & 0 & 0 \\ 0 & 1 & 0 & 0 \\ 0 & 0 & 1 & 0 \\ 0 & 0 & 0 & i \end{bmatrix}$
- **Toffoli gate** (3-qubit, CCNOT): 8×8 matrix with $U_{\text{Toffoli}}|abc\rangle = |ab(c \oplus ab)\rangle$ for $a, b, c \in \{0, 1\}$, swapping $|110\rangle$ and $|111\rangle$
- **Fredkin gate** (3-qubit, controlled-SWAP): 8×8 matrix with $U_{\text{Fredkin}}|abc\rangle = |a\rangle|cb\rangle$ if $a = 1$, else $|abc\rangle$, conditionally swapping qubits 2 and 3

For each gate U , we construct noisy implementations V via mixed unitary channels $V(\rho) = \sum_k p_k V_k \rho V_k^\dagger$ with noise unitaries $\{V_k\}$ representing three common error sources: bit-flip errors (X rotations), phase errors (Z rotations), and depolarizing noise (random Pauli errors). Using our trained ML model, we compute $e(U, V) = \frac{1}{n} \max_\rho \|U\rho U^\dagger - V(\rho)\|_{W_1}$ for each gate-noise combination.

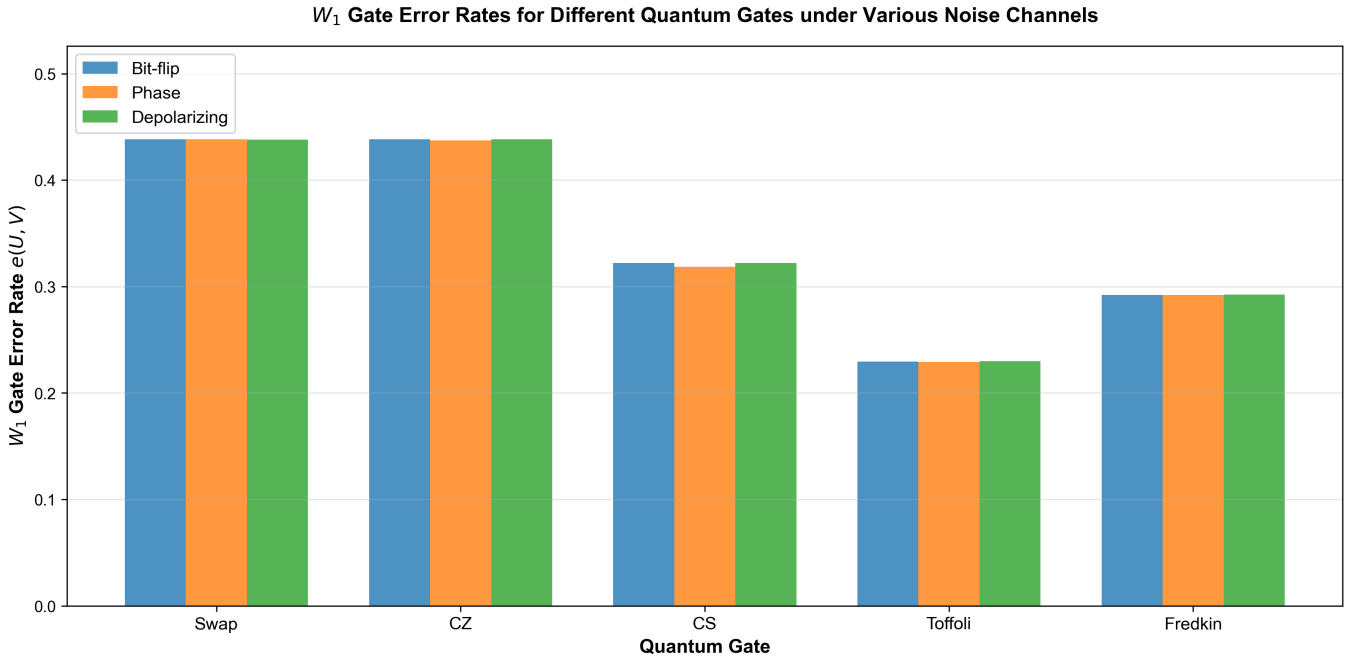


FIG. 5: W_1 gate error rates $e(U, V)$ for different quantum gates under various noise channels, computed using our ML model. The results reveal gate-specific noise sensitivity: Swap gate is more robust to bit-flip noise but sensitive to phase errors, while CZ gate shows the opposite pattern. Multi-qubit gates (Toffoli, Fredkin) exhibit distinct error rate profiles.

Figure 5 presents the computed error rates, revealing gate-specific noise sensitivity patterns: (1) **Swap gate**: More robust to bit-flip noise but sensitive to phase errors, reflecting its role in state exchange rather than phase manipulation. (2) **CZ and CS gates**: Show opposite sensitivity—CZ is robust to phase errors but sensitive to bit-flip noise, while CS exhibits similar phase-robust characteristics, consistent with their phase-dependent operations. (3) **Multi-qubit gates**: Toffoli and Fredkin gates show distinct error rate profiles, with Toffoli being particularly sensitive to correlated errors affecting multiple control qubits. These results demonstrate that $e(U, V)$ provides a physically meaningful metric for identifying which gates are robust or vulnerable to specific noise types, enabling targeted error correction strategies. Our ML framework enables efficient computation of $e(U, V)$ for larger gates where traditional numerical methods become computationally prohibitive.

VI. DISCUSSION

We have presented the first systematic machine learning framework for predicting quantum Wasserstein distances, addressing a fundamental challenge in quantum information theory. Our approach combines comprehensive feature extraction from quantum state pairs with both classical neural networks and traditional machine

learning models. The feature set encompasses Pauli measurements (4^{n+1} features), statistical moments, quantum fidelity, entanglement measures (von Neumann entropy, linear entropy, relative entropy), eigenvalue statistics, and partial trace features for multi-qubit systems.

Our experimental results demonstrate exceptional prediction accuracy: the best-performing Random Forest model achieves near-perfect performance ($R^2 = 0.9999$) on three-qubit systems, with mean absolute errors on the order of 10^{-5} . Tree-based models consistently outperform linear models, indicating a highly nonlinear relationship between quantum state features and W-distance. However, linear models still achieve excellent performance ($R^2 \approx 0.9992$), suggesting that a significant portion of the W-distance can be approximated through linear combinations of features. The high pairwise correlation (> 0.99) between predictions from different model architectures confirms the robustness of the learned relationship.

Beyond prediction accuracy, we validate the practical utility of our ML framework by applying it to verify two fundamental theoretical propositions in quantum information theory. First, we used model-predicted distances to validate Proposition 1, which bounds the measurement probability difference between unitary operations by the quantum W_1 distance. Across 300 Monte Carlo trials, we observed no violations of the theoretical bound, with maximum ratios ≤ 0.95 , demonstrating that our ML model preserves essential theoretical guarantees.

Second, we validate Proposition 2, which relates the W_1 gate error rate to the average cost of recovery operations in quantum error correction. Using 200 Monte Carlo trials on 2-qubit systems, our ML model successfully validated the theoretical upper bound with no violations observed. The model's prediction error (MSE $\sim 10^{-6}$, MAE $\sim 10^{-4}$) is sufficiently small to enable reliable theoretical validation in practical scenarios where exact computation may be computationally expensive.

These validation experiments establish that machine learning can serve not only as a computational tool but also as a reliable method for verifying theoretical bounds in quantum information theory, opening new avenues for combining data-driven approaches with rigorous theoretical analysis.

Several limitations of our current framework should be addressed in future work:

- 1. System scalability:** Our experiments focus on systems up to four qubits. Extending to larger systems (5+ qubits) will require addressing the exponential growth in feature dimension and potential overfitting. Feature selection techniques and dimensionality reduction methods could help mitigate this challenge.
- 2. Hybrid quantum-classical models:** The current framework uses only classical machine learning. Integrating parameterized quantum circuits (PQCs) for

feature extraction could potentially leverage quantum advantages and improve performance on larger systems, while also reducing computational overhead.

3. **Noise robustness:** While our framework handles various state types, explicit noise robustness testing on experimental quantum hardware would strengthen practical applicability in NISQ devices.
4. **Analytical validation:** For specific gate pairs with known analytical W-distances, we should validate that our predictions match theoretical values to ensure accuracy across different operation types.
5. **Real-time applications:** Future work should explore optimization techniques for real-time quantum circuit assessment and error correction protocol design, where computational efficiency is critical.

VII. CONCLUSION

This work establishes machine learning as a viable and scalable alternative to traditional numerical methods for quantum W-distance computation. The combination of physically meaningful feature extraction, high prediction accuracy, and successful theoretical validation demonstrates the potential of data-driven approaches in quantum information theory. The framework shows particular promise for real-time quantum circuit assessment and error correction protocol design in NISQ devices, where efficient distance quantification is urgently needed.

The success of this approach opens new avenues for applying machine learning to other challenging quantum information tasks, such as quantifying entanglement, characterizing quantum channels, and optimizing quantum error correction codes. As quantum technologies continue to advance, the integration of machine learning with rigorous theoretical analysis will play an increasingly important role in bridging the gap between theoretical understanding and practical quantum applications.

VIII. ACKNOWLEDGMENTS

This study was supported by the National Natural Science Foundation of China (Grant Nos. 11871089, 12471427, 52472442, 72471013 and 62103030), the Research Start-up Funds of Hangzhou International Innovation Institute of Beihang University (Grant Nos. 2024KQ069, 2024KQ036 and 2024KQ035) and the Postdoctoral Research Funding of Hangzhou International Innovation Institute of Beihang University (Grant No.2025BKZ066).

IX. DATA AVAILABILITY STATEMENT

All data that support the findings of this study are included within the article (and any supplementary files).

X. DECLARATION OF COMPETING INTEREST

The authors declare that they have no known competing financial interests or personal relationships that could have appeared to influence the work reported in this paper.

Appendix A: Computational Complexity and 4-Qubit Implementation Notes

Scaling from $n = 2$ to $n = 4$ incurs significant computational overhead due to matrix dimension $d = 2^n$ and the size of the Pauli basis. Table below summarizes the dominant costs:

Component	Cost (per evaluation)	$n = 2$	$n = 3$	$n = 4$
W_1 (trace-distance approximation)	$O(d^3)$	$O(d^3)$	$O(4^3)$	$O(16^3)$
Pauli features (4^{n+1} ops, each $\sim O(d^2)$)	$O(16^n)$	$O(16^2)$	$O(16^3)$	$O(16^4)$
Fidelity (matrix square roots)	$O(d^3)$	$O(4^3)$	$O(8^3)$	$O(16^3)$

Empirically, this leads to an order-of-magnitude slow-down from $n = 2$ to $n = 4$ for data generation and feature extraction. Practical remedies include:

- Active generation via binary search over mixing parameters to reduce attempts.
- Parallelized sample generation and cached Pauli bases.
- Faster eigensolvers or approximate spectra for large d .
- Lightweight feature selection and stronger learners to reduce input dimension while preserving accuracy.

[1] S. Jerbi, C. Gyurik, S. C. Marshall, et al. Shadows of quantum machine learning. *Nature Communications*, 15:5676, 2024.
[2] Yi-Jun Luo, Jin-Ming Liu, and Chengjie Zhang. Detecting genuine multipartite entanglement via machine learning. *Phys. Rev. A*, 108:052424, Nov 2023.
[3] Cornish S.L., Tarbutt M.R., and Hazzard K.R.A. Quantum computation and quantum simulation with ultracold molecules. *Nat. Phys.*, 20:730–740, 2024.
[4] Martin Larocca, Frederic Sauvage, Faris M. Sbahi, Guillaume Verdon, Patrick J. Coles, and M. Cerezo. Group-invariant quantum machine learning. *PRX Quantum*, 3:030341, Sep 2022.
[5] Lifeng Zhang, Zhihua Chen, and Shao-Ming Fei. Entanglement verification with deep semisupervised machine learning. *Phys. Rev. A*, 108:022427, Aug 2023.

- [6] Yunfei Wang and Junyu Liu. A comprehensive review of quantum machine learning: from nisq to fault tolerance. *Rep. Prog. Phys.*, 87:116402, 2024.
- [7] Yang Dong, Shao-Chun Zhang, Yu Zheng, Hao-Bin Lin, Long-Kun Shan, Xiang-Dong Chen, Wei Zhu, Guan-Zhong Wang, Guang-Can Guo, and Fang-Wen Sun. Experimental implementation of universal holonomic quantum computation on solid-state spins with optimal control. *Phys. Rev. Appl.*, 16:024060, 2021.
- [8] K. Beer, D. Bondarenko, et al. Training deep quantum neural networks. *Nature Communications*, 11:808, 2020.
- [9] Erik Recio-Armengol, Jens Eisert, and Johannes Jakob Meyer. Single-shot quantum machine learning. *Phys. Rev. A*, 111:042420, 2025.
- [10] David Peral-Garcia, Juan Cruz-Benito, and Francisco Jose Garcia-Penalvo. Systematic literature review: Quantum machine learning and its applications. *Computer Science Review*, 51:100619, 2024.
- [11] Biamonte J., Wittek P., Pancotti N., et al. Quantum machine learning. *Nature*, 549:195–202, 2017.
- [12] A. Acin. Statistical distinguishability between unitary operations. *Phys. Rev. Lett.*, 87:177901, 2001.
- [13] Xinyu Qiu, Lin Chen, and Li-Jun Zhao. Quantum wasserstein distance between unitary operations. *Phys. Rev. A*, 110:012412, 2024.
- [14] Giacomo De Palma, Milad Marvian, Dario Trevisan, and Seth Lloyd. The quantum wasserstein distance of order 1. *IEEE Transactions on Information Theory*, 67(10):6627–6643, 2021.
- [15] Emily Beatty and Daniel Stilck Franca. Order p quantum wasserstein distances from couplings. *Annales Henri Poincare*, 2025.
- [16] Easwar Magesan, Jay M. Gambetta, A. D. Córcoles, and Jerry M. Chow. Machine learning for discriminating quantum measurement trajectories and improving readout. *Phys. Rev. Lett.*, 114:200501, 2015.
- [17] Kyriaki A. Tychola, Theofanis Kalampokas, and George A. Papakostas. Quantum machine learning—an overview. *Electronics*, 12(11), 2023.
- [18] Ciliberto Carlo, Herbster Mark, et al. Quantum machine learning: a classical perspective. *Proc. R. Soc. A.*, 474:20170551, 2018.
- [19] Xiaodie Lin, Zhenyu Chen, and Zhaohui Wei. Quantifying quantum entanglement via a hybrid quantum-classical machine learning framework. *Phys. Rev. A*, 107:062409, 2023.
- [20] Changchun Feng and Lin Chen. Quantifying quantum entanglement via machine learning models. *Communications in Theoretical Physics*, 76(7), 2024.
- [21] David E. Rumelhart, Geoffrey E. Hinton, and Ronald J. Williams. Learning representations by back-propagating errors. *Nature*, 323(6088):533–536, 1986.
- [22] Geoffrey E. Hinton, Simon Osindero, and Yee Whye Teh. A fast learning algorithm for deep belief nets. *Neural Computation*, 18(7):1527–1554, 2006.
- [23] Maria Schuld, Ilya Sinayskiy, and Francesco Petruccione. Supervised learning with quantum neural networks on a near-term processor. *Physical Review Letters*, 122(4):040504, 2019.
- [24] Marcello Benedetti, Edward Lloyd, Alejandro Perdomo-Ortiz, John Realpe-Gómez, and Jochen Braumüller. Parameterized quantum circuits as machine learning models. *Physical Review Research*, 1(2):023024, 2019.
- [25] Alex Krizhevsky, Ilya Sutskever, and Geoffrey E. Hinton. Imagenet classification with deep convolutional neural networks. *Commun. ACM*, 60(6):84–90, May 2017.
- [26] J. Ross Quinlan. Induction of decision trees. *Machine Learning*, 1(1):81–106, 1986.
- [27] Leo Breiman. Random forests. *Machine Learning*, 45(1):5–32, 2001.
- [28] Robert E Schapire Yoav Freund. A decision-theoretic generalization of on-line learning and an application to boosting. *Computational Learning Theory*, 55(1):119–139, 1997.
- [29] Richard A. Berk. *Statistical Learning as a Regression Problem[M]*, pages 1–48. Springer New York, New York, NY, 2008.
- [30] Hailan Ma, Bo Qi, Ian R Petersen, Re-Bing Wu, Herschel Rabitz, and Daoyi Dong. Machine learning for estimation and control of quantum systems. *National Science Review*, 12(8):nwaf269, 07 2025.
- [31] Vaclav Havlicek, Alba Cervera-Lierta, Thibaut H. Kyaw, Kristan Temme, Aram W. Harrow, Abhinav Kandala, Jerry M. Chow, and John M. Martinis. Supervised learning with quantum-enhanced feature spaces. *Nature*, 567(7747):209–213, 2019.
- [32] Patrick Rebentrost, Masoud Mohseni, and Seth Lloyd. Quantum support vector machines for big data classification. *Physical Review Letters*, 113(13):130503, 2014.
- [33] Jiaye Li, Yangding Li, Jiagang Song, Jian Zhang, and Shichao Zhang. Quantum support vector machine for classifying noisy data. *IEEE Transactions on Computers*, 73(9):2233–2247, 2024.
- [34] Kilian Tscharke, Sebastian Issel, and Pascal Debus. Semisupervised anomaly detection using support vector regression with quantum kernel. In *2023 IEEE International Conference on Quantum Computing and Engineering (QCE)*, volume 01, pages 611–620, 2023.